

Void containing AlN layer grown on AlN nanorods fabricated by polarity selective epitaxy and etching method

Cite as: AIP Advances **11**, 045036 (2021); <https://doi.org/10.1063/5.0042631>

Submitted: 01 January 2021 • Accepted: 23 February 2021 • Published Online: 30 April 2021

 Byeongchan So, Junchae Lee, Changheon Cheon, et al.

COLLECTIONS

 This paper was selected as Featured



View Online



Export Citation



CrossMark

ARTICLES YOU MAY BE INTERESTED IN

[Strain management and AlN crystal quality improvement with an alternating V/III ratio AlN superlattice](#)

Applied Physics Letters **118**, 262101 (2021); <https://doi.org/10.1063/5.0048656>

[AlGaIn-based deep UV LEDs grown on sputtered and high temperature annealed AlN/sapphire](#)

Applied Physics Letters **112**, 041110 (2018); <https://doi.org/10.1063/1.5010265>

[Suppression of dislocation-induced spiral hillocks in MOVPE-grown AlGaIn on face-to-face annealed sputter-deposited AlN template](#)

Applied Physics Letters **116**, 062101 (2020); <https://doi.org/10.1063/1.5141825>



Call For Papers!

AIP Advances

SPECIAL TOPIC: Advances in Low Dimensional and 2D Materials

Void containing AlN layer grown on AlN nanorods fabricated by polarity selective epitaxy and etching method

Cite as: AIP Advances 11, 045036 (2021); doi: 10.1063/5.0042631

Submitted: 1 January 2021 • Accepted: 23 February 2021 •

Published Online: 30 April 2021



View Online



Export Citation



CrossMark

Byeongchan So,¹  Junchae Lee,¹ Changheon Cheon,¹ Joohyung Lee,¹  Uiho Choi,¹  Minho Kim,¹ Jindong Song,² Joonyeon Chang,²  and Okhyun Nam^{1,a)} 

AFFILIATIONS

¹CANS (Convergence Center for Advanced Nano Semiconductor), Department of Nano & Semiconductor Engineering, Korea Polytechnic University, 237 Sangidaehakro, Siheung, Gyeonggi-do 15073, Republic of Korea

²Post-Silicon Semiconductor Institute, Korea Institute of Science and Technology (KIST), Hwarang-ro 14 gil, Seongbuk-gu, Seoul 02792, Republic of Korea

^{a)} Author to whom correspondence should be addressed: ohnam@kpu.ac.kr

ABSTRACT

Creating voids between thin films is a very effective method to improve thin film crystal quality. However, for AlN material systems, the AlN layer growth, including voids, is challenging because of the very high Al atom sticking coefficient. In this study, we demonstrated an AlN template with many voids grown on AlN nanorods made by polarity selective epitaxy and etching methods. We introduced a low V/III ratio and NH₃ pulsed growth method to demonstrate high-quality coalesced AlN templates grown on AlN nanorods in a metal organic chemical vapor deposition reactor. The crystal quality and residual strain of AlN were enhanced by the void formations. It is expected that this growth method can contribute to the demonstration of high-performance deep UV LEDs and transistors.

© 2021 Author(s). All article content, except where otherwise noted, is licensed under a Creative Commons Attribution (CC BY) license (<http://creativecommons.org/licenses/by/4.0/>). <https://doi.org/10.1063/5.0042631>

Recently, the world has faced a terrible epidemic because of the coronavirus (COVID-19), which spreads from person-to-person, mostly through respiratory droplets that occur when an infected individual sneezes or coughs in the air.^{1,2} Chemical methods are primarily used to prevent the virus from spreading, but there is a limit of their use in large spaces and crowded areas.³ AlGaIn-based deep ultraviolet light-emitting diodes (DUV LEDs) are promising sterilization and decontamination candidates to prevent epidemics.⁴⁻⁶ However, the performance of AlGaIn-based DUV LEDs needs to be improved for general use in virus disinfection. There are several problems blocking performance improvement of DUV LEDs as sterilization light sources. One problem is the non-radiative recombination in multi-quantum wells (MQWs) due to the high dislocation density caused by the difference in the large lattice mismatch and the thermal expansion coefficient between the AlN layer and the sapphire substrate, which induces low internal quantum efficiency (IQE).⁷⁻⁹ The poor carrier injection efficiency (CIE) is another problem that hinders performance improvement of DUV LEDs.^{10,11} The

ultrawide bandgap (3.4–6.2 eV) of AlGaIn-based materials has inherently high dopant activation energy in both *n*- and *p*-type, making high-efficiency doping very challenging in this material system.^{12,13} In addition, the light extraction efficiency (LEE) is decreased because the DUV light emitted from AlGaIn MQWs is partially absorbed by the *p*-cladding layer.¹⁴ One of the most effective methods to solve low efficiency issue in DUV LEDs is to grow high-quality AlN templates because low defect AlN not only affects the enhancement of IQE but also improves the doping efficiency of the upper cladding layer.⁹ Some groups have attempted to study a patterned sapphire substrate (PSS), epitaxial lateral overgrowth (ELO), sputtered AlN and nanostructures to reduce the dislocation density in the AlN layer.¹⁵⁻¹⁹ However, in AlN material systems, ELO using a selective mask, being very favorable for void generation in the GaN material system, is limited owing to the high Al atom sticking coefficient.²⁰ Therefore, mask-assist growth and void formation in AlN-based materials are very circumscribed, as compared with GaN materials.^{21,22}

To overcome these fundamental limitations, in this study, we used AlN nanorods fabricated by the polarity selective epitaxy and etching (PSEE) method for the growth of AlN layers embedded with numerous voids.²³ The voids were primarily formed at the interface between the regrown AlN layer and AlN nanorods. The PSEE method has been studied for high-efficiency DUV emitters in our group by high-temperature metal organic chemical vapor deposition (HT-MOCVD).²⁴ The surface morphology of regrown AlN on AlN nanorods was practically merged, and the crystal quality was improved by controlling the regrowth conditions in the MOCVD reactor. In addition, this approach is expected to be an alternative technique to enhance the crystal quality of the AlN template using only the MOCVD system because it does not include any complicated fabrication processes, such as photolithography and nanoimprint technology for making selective masks.²⁵

The growth process for the two AlN layer types is described in Fig. 1. Conventional Al-polar AlN and polarity selective epitaxial (PSE) AlN were grown on a 0.2° off-angle c-plane sapphire substrate (diameter: 2 in.) using the HT-MOCVD (Top Engineering, PHAETHON 100U) system. H₂ thermal cleaning was performed on the sapphire substrate in the MOCVD reactor before AlN growth. The H₂ annealing temperature on the sapphire substrate was varied to control the AlN polarity. The growth schematic diagram shown in Fig. 1 describes that the H₂ annealing temperatures were 1075 °C and 1250 °C for conventional AlN and PSE AlN, respectively.²⁴ Subsequently, the low-temperature (LT) AlN buffer layers with 25 and 5 nm were grown on thermally cleaned sapphire to stack conventional AlN and PSE AlN, respectively.²⁶ Finally, 2 μm AlN layers were grown at 1250 °C for 3600 s on both buffer layer types.

After growth, the PSE AlN was chemically etched using a 2.5 wt. % potassium hydroxide (KOH) solution at 80 °C for 10 and 30 s. The different AlN nanorods were formed using the KOH chemical etching method by inducing the preferential etching process of the N-polar region of PSE AlN.²⁷ For improved AlN growth, AlN was regrown on the AlN nanorods fabricated by the PSEE method using the MOCVD system. The AlN regrowth condition was controlled by changing the V/III ratio from 300 to 10 and introducing 45 pairs of pulsed gas injection epitaxy at 1250 °C in the MOCVD reactor.

One pair of pulsed epitaxy consists of simultaneous source injection of group III and V sources for 3 s and interruption of the group V source for 5 s. During the AlN growth process, the reactor pressure was maintained at 4 kPa. Trimethylaluminum (TMA) and ammonia (NH₃) were used as Al and N sources, respectively.

A scanning electron microscope (SEM) was used to observe the surface morphology and cross-sectional image of AlN using the SEM system (S-4000, Hitachi). A high resolution x-ray diffraction (HR-XRD) system (X'Pert Pro MRD cradle, Panalytical) with a Cu-Kα target ($\lambda = 1.54 \text{ \AA}$) was used to observe the crystal quality of AlN using the x-ray rocking curve (XRC) method. Cathodoluminescence (CL) analysis of AlN was performed using the CL system (MONO CL3+, GATAN). The selective area electron diffraction (SAED) and dislocation behavior of the AlN layer were measured by using a cross-sectional transmission electron microscopy (TEM) system (JEOL, JE-2100F). Raman spectroscopy with a laser excitation source at a wavelength of 532 nm was used to measure the optical AlN characteristics at room temperature. An atomic force microscope (AFM) system (XE-7, Park systems) in non-contact mode was used to observe the surface morphology of the AlN layer.

The polarity of the AlN layer is controlled by the initial growth condition on the sapphire substrate in the MOCVD reactor, as shown in Fig. 1. We introduced a high-temperature (1250 °C) H₂ annealing and nitridation step to obtain mixed-polarity AlN seeds. The surface bonding of the sapphire substrate was modified from Al-O to Al-N-O by introducing H₂ annealing and nitridation processes at 1250 °C.²⁴ Finally, a thin buffer layer (~5 nm) induced the formation of mixed polarity seeds to demonstrate a mixed polar AlN layer.²⁶ The SEM images show the surface morphologies of conventional AlN and PSE AlN grown under different pre-treatment conditions, as shown in the inset of Fig. 1. The conventional AlN shows a very smooth surface morphology, but PSE AlN has a rough surface morphology.²⁷

Figures 2(a)–2(c) show the SEM plan-view images of PSE AlN depending on the KOH etching time. The surface morphology of PSE AlN consists of numerous Al-polar AlN domains with different sizes (100–400 nm). The inversion main boundary region was preferentially etched after KOH immersion for 10 s, which is caused

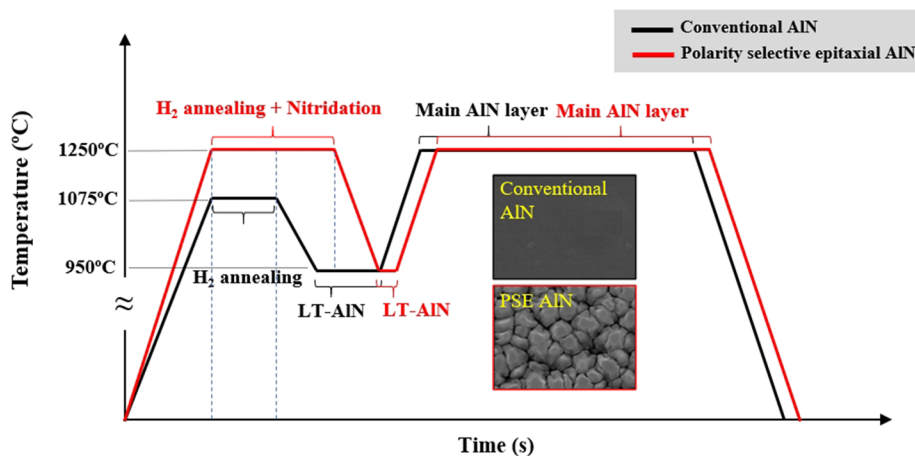


FIG. 1. Growth procedures and SEM surface images for conventional and PSE AlN, respectively.

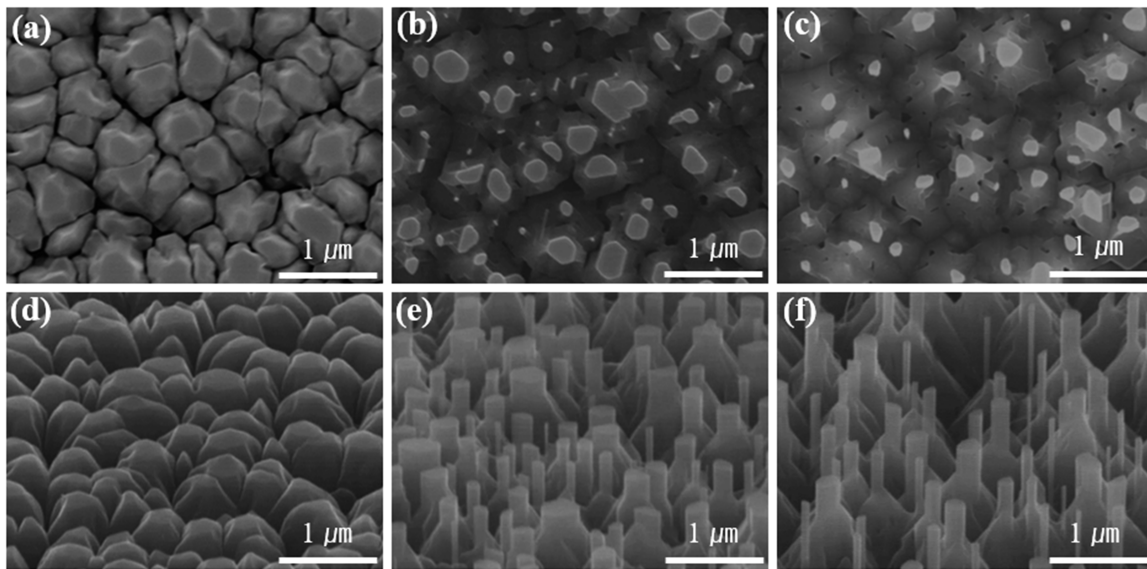


FIG. 2. SEM surface morphology and bird's eye view images of PSE AlN etched for (a) and (d) 0 s, (b) and (e) 10 s, and (c) and (f) 30 s, respectively.

by the difference in the etch rate between Al- and N-polar AlN.²³ The SEM bird's eye view shows that the AlN nanorods were formed by KOH wet etching, as shown in Figs. 2(d)–2(f). As the etching time increased to 30 s, the AlN domain size decreased, and the aspect ratio increased. However, the XRC FWHM of AlN etched with KOH for 30 s was increased by decreasing the Al-polar domain region, as indicated in Table I. This increase in the XRC FWHM in the KOH 30 s sample implies that etching time exceeding a critical point excessively reduces the volume of the Al-polar region of the AlN nanorods, which is also proved through decreased domain size of Al-polar AlN, as shown in Fig. 2(c). Finally, we used AlN nanorods with KOH for 10 s as the template for demonstration of high-quality AlN.

Figures 3(a)–3(d) show the plan-view images of 10 s etched PSE AlN and 3600 s regrown AlN depending on the different growth conditions by observing SEM measurement. Figure 3(b) indicates a non-coalescent surface of the AlN layer grown by the conventional growth AlN condition (V/III ratio: 300). Generally, it is reported that the high V/III ratio promotes the three-dimensional growth mode during AlN growth in the MOCVD system.²⁸ To achieve the merged surface of AlN, we changed the V/III ratio to 10 during the AlN regrowth process. Figure 3(c) shows the nearly coalesced surface morphology of AlN, which is assumed that the lateral growth was induced by a low V/III ratio. However, the pits were formed on the AlN surface by insufficient merge under a V/III

ratio of 10. Therefore, we inserted a layer that significantly promotes lateral growth by pulsed NH₃ injection near the top region of the AlN nanorods before the continuous regrowth step. The regrown AlN surface was merged in the end by introducing pulsed growth and a low V/III ratio, as shown in Fig. 3(d). The cross-sectional SEM images in Figs. 3(e)–3(h) show the 10 s etched PSE AlN and 3600 s regrown AlN depending on different growth conditions, which including voids formed at the interface between the bottom region of regrown AlN and the top region of the AlN nanorods.

The AlN thickness varied depending on the regrowth condition. Figure 3(e) shows the thickness of KOH-etched AlN at $\sim 2 \mu\text{m}$. The regrown AlN with a V/III ratio of 300 has a thickness of $4 \mu\text{m}$ because the growth condition was the same between PSE AlN nanorods and regrown AlN, as indicated in Fig. 3(f). However, the thickness of regrown AlN with a V/III ratio of 10 was increased $\sim 5 \mu\text{m}$ by reducing the NH₃ source gas, as shown in Fig. 3(g). Finally, the thickness of AlN regrown with pulsed growth and a V/III ratio of 10 was about $5.5 \mu\text{m}$, as shown in Fig. 3(h). The slight increase in AlN thickness is due to the insertion of the NH₃ pulsed growth layer. These results suggest that the low V/III ratio AlN growth developed not only the lateral AlN growth on nanorods but also the AlN growth rate.²⁹

Table II shows the XRC FWHMs of the regrown AlN samples. The (002) XRC FWHMs of regrown AlN increased, as compared to that of AlN NRs, from 250 to 320 arc sec. This means that the screw dislocations increased during the AlN regrowth process.³⁰ However, the (102) XRC FWHMs differed depending on the regrowth condition, as shown in Table II. In particular, the (102) XRC FWHM of AlN regrown with the pulsed step and a V/III ratio of 10 was reduced, as compared to PSE AlN, from 470 to 425 arc sec. It is assumed that lateral overgrowth by the pulsed step induced blocking and bending of dislocations. Therefore, the dislocations could not reach the top surface region of regrown AlN. It was reported that

TABLE I. The XRC FWHMs of PSE AlN etched for 0, 10, and 30 s.

Sample	(002) FWHM (Arc sec)	(102) FWHM (Arc sec)
Before KOH	220	470
KOH 10 s	250	470
KOH 30 s	325	500

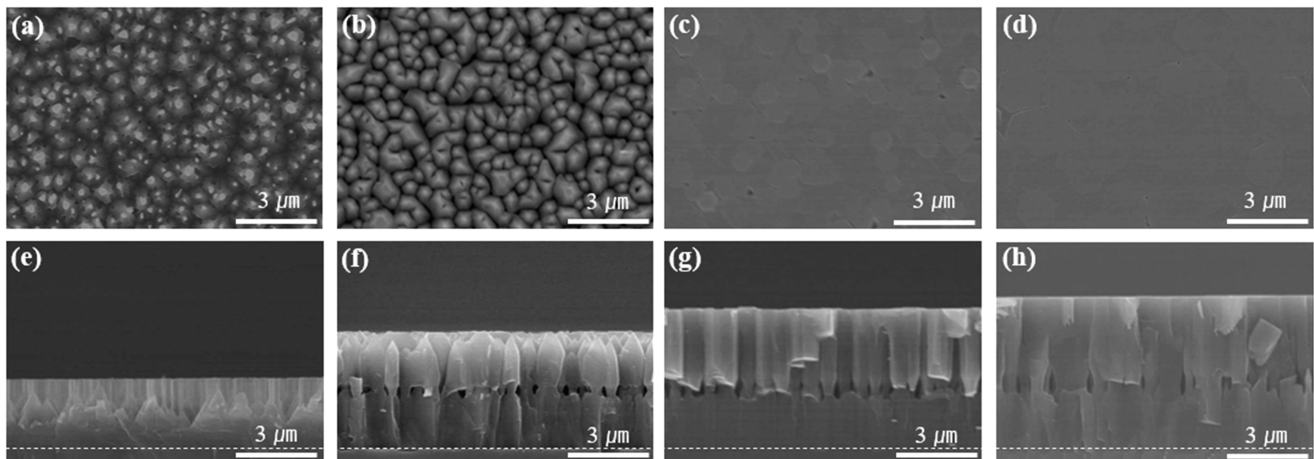


FIG. 3. SEM surface morphology and cross-sectional images of (a) and (e) 10 s etched AlN and 3600 s regrown AlN under conditions of (b) and (f) V/III ratio 300, (c) and (g) 10, and (d) and (h) 10 with pulsed growth, respectively. White dash lines indicate the interface between AlN and the sapphire substrate.

the (102) XRC FWHM is closely affected by the edge type threading dislocation, according to Heying *et al.*, and therefore, the rocking curve widths for (102) are more reliable factors of crystal quality.³¹ In addition, it is very sensitive to the performance of nitride-based devices.³²

Figure 4 shows the schematic procedure for the fabrication of PSEE AlN nanorods and regrowth of AlN depending on the regrowth condition. First, the PSEE AlN was grown by introducing high-temperature H₂ cleaning on sapphire and a 5 nm AlN buffer layer, which consists of different Al- and N-polar AlN domains, as shown in Fig. 4(a). Subsequently, the PSEE AlN was chemically wet etched using a KOH solution. The AlN nanorods were fabricated by the difference in the etch rate between Al- and N-polarity, as shown in Fig. 4(b).³³ In our early work, we used the PSEE AlN nanorod structure and demonstrated a high-efficiency DUV emitter based on this method.²⁴ Figures 4(c)–4(f) show the AlN regrowth behavior by changing the growth conditions. Figure 4(c) indicates the regrown AlN with a V/III ratio of 300, which is the conventional AlN layer growth condition in our MOCVD system. Judging from the SEM cross-sectional view, the change to a low V/III ratio affects the growth behavior of AlN, as shown in Fig. 4(d). It is assumed that the AlN growth proceeded in both polarities and the growth rate gap between Al-polar and N-polar is larger, similar to decreasing the V/III ratio seen in the void shapes. Consequently, the shape of the voids in regrown AlN tends to become horizontally narrower

and vertically longer. To further promote surface coalescence, at the very first stage of AlN regrowth, we introduced pulsed NH₃ injection growth, as shown in Fig. 4(e). The NH₃ gas was periodically injected and stopped for 45 pairs with continuous TMA flow. Subsequently, AlN was regrown for 3600 s on the pulsed grown AlN layer as the second step. Finally, a fully coalesced AlN layer with many voids was demonstrated, as shown in Fig. 4(f). Given the regrowth behavior, the low V/III ratio, which means decreased NH₃ gas flow, preferentially induces the overgrowth of AlN at the top region of the Al-polarity nanorods. Furthermore, the introduction of the pulsed layer additionally promoted surface coalescence and crystal quality of AlN.³⁴ The AlN thickness is ~5.5 μm. The total AlN thickness is relatively thinner than those of the other groups that have used the nano-patterned sapphire substrate, and therefore, there is room to increase the thickness for high crystal quality AlN.³⁵

Figure 5 shows the characterization of regrown AlN with pulsed and a V/III ratio of 10 in the cross-sectional position. Figures 5(a) and 5(b) show the SEM cross-sectional images of regrown AlN, which correspond with the CL spectra measured under an acceleration voltage of 5 kV, as shown in Fig. 5(c). We observed only the deep-level emission of regrown AlN from 250 nm because of the wavelength limitation of the CL system. The CL spectra were measured between 300 and 500 nm at three points consisting of above the voids (region A), near the voids (region B), and beneath the voids (region C), as indicated in Figs. 5(a) and 5(b),

TABLE II. The XRC FWHMs of PSEE AlN and regrown AlN depending on the growth conditions.

Sample	(002) FWHM (Arc sec)	(102) FWHM (Arc sec)
PSEE NRs	250	470
Regrowth	320	560
Regrowth	320	430
Regrowth	310	425

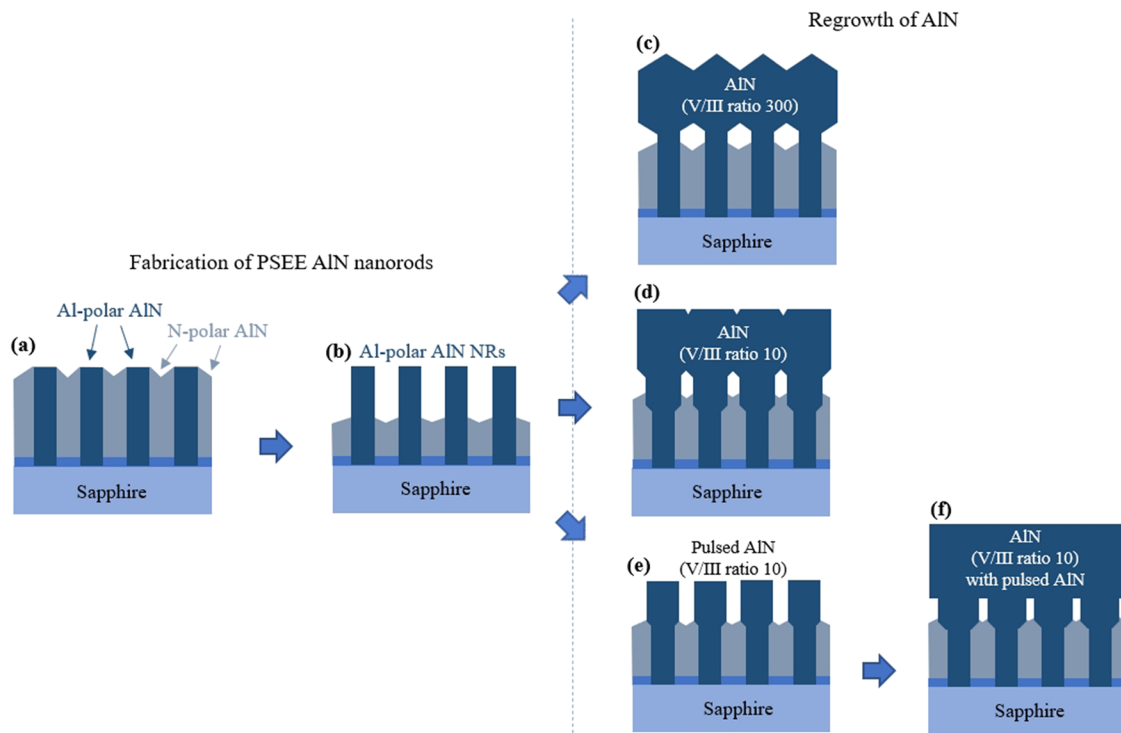


FIG. 4. Schematic illustration of the growth process for PSEE AlN nano-rods and regrown AlN samples. (a) and (b) indicate the fabrication of PSE AlN and PSEE AlN NRs. The epitaxial growth mechanisms of regrown AlN samples depending on the V/III ratio are shown in (c)–(f).

respectively. The origin of these peaks was attributed to the oxygen-related impurities ($V_{Al}-O_N$ and $V_{Al}-2O_N$), but further studies are needed to establish the exact origin.³⁶ These deep-level emissions were reduced with increasing growth thickness of regrown AlN, as shown in Fig. 5(c). In particular, the impurity

emissions were nearly eliminated at the top AlN region. Figure 5(d) shows a cross-sectional TEM image with a zone axis of [1-100] shows a high density of dislocations near the interface between the AlN and sapphire. A two-beam condition with a g-vector (11-20) was used to observe the behavior of edge and mixed dislocations.

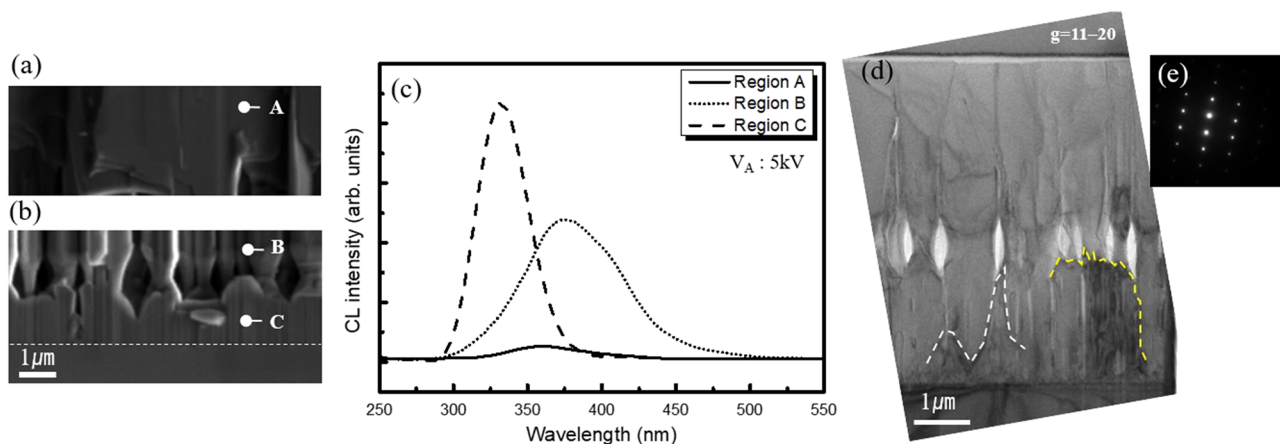


FIG. 5. Characterization of regrown AlN with pulsed growth and a V/III ratio of 10 in the cross-sectional position. SEM cross-sectional images of the region for (a) regrown AlN and (b) AlN nano-rods and the interface between AlN and the sapphire substrate. (c) CL spectra in accordance with positions in SEM images. (d) The TEM cross-sectional image of regrown AlN with the zone axis [1-100] under the two-beam condition. (e) The SAED patterns of regrown AlN.

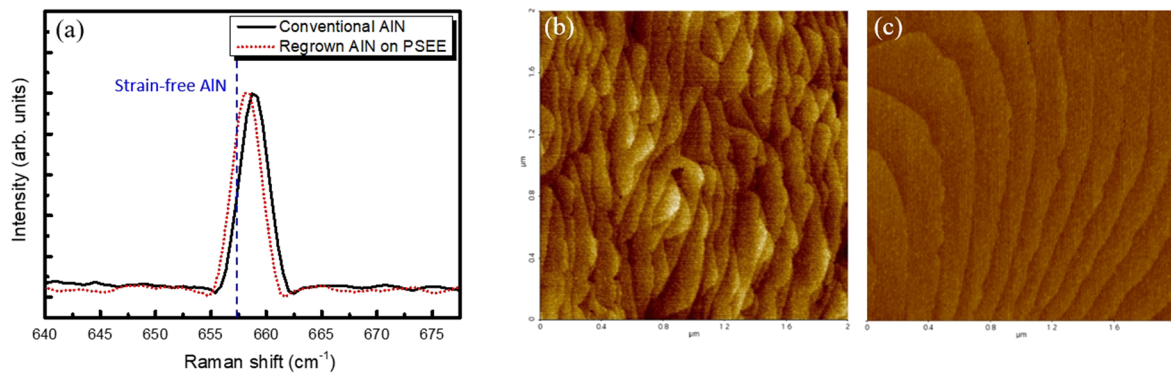


FIG. 6. Characterizations of conventional AlN and regrown AlN with pulsed growth and a V/III ratio of 10. (a) Raman spectra of conventional AlN and regrown AlN. The AFM images of (b) conventional AlN and (c) regrown AlN.

However, the upper region of the void shows a significantly reduced dislocation density. We observed two dislocation reduction mechanisms in regrown AlN using TEM analysis. First, the white dotted line indicates the controlled dislocation during the PSE growth process. Our previous study reported that the Al-polar region inherently has low dislocation densities, as compared with the N-polar region in mixed-polarity AlN.²³ The other dislocation reduction mechanism in regrown AlN is indicated by the yellow dotted line. The dislocations are blocked by voids, which are formed during the AlN regrowth process. Therefore, the upper AlN of voids region shows considerably reduced dislocations, as compared with the lower region. Figure 5(e) shows the SAED pattern of the regrown AlN. The SAED pattern taken from the top AlN region indicates a clear hexagonal pattern.

Figure 6 shows the comparison results of Raman and AFM between the conventional AlN and AlN regrown on the PSEE nanorods. The XRC FWHMs of conventional AlN are 240 and 460 arc sec for (002) and (102), respectively, whose values are similar to those of AlN regrown on PSEE nanorods. The Raman spectra of the conventional AlN and AlN regrown on the PSEE nanorods were measured, as shown in Fig. 6(a). The peak E^2 (high) phonon frequencies of the conventional AlN and AlN regrown on the PSEE are 659.2 and 658 cm^{-1} , respectively. It was reported by Prokofyeva that the phonon frequency of strain-free AlN is 657.4 cm^{-1} for the E^2 (high) phonon mode.³⁷ The Raman phonon peaks related to the AlN sample types were shifted to the higher-frequency side than those of the strain-free AlN. These peak shifts were caused by residual compressive strain because of mismatches in the thermal expansion coefficient between AlN and the sapphire substrate.³⁸ The E^2 (high) phonon frequency peak of the AlN grown on PSEE was 658 cm^{-1} , which is closer to the strain-free AlN than planar AlN. These results suggest that the compressive strain in AlN grown on PSEE NR is relaxed by void formation.³⁹ Figures 6(b) and 6(c) show the AFM surface morphology of conventional AlN and regrown AlN on PSEE. A step terrace surface was observed in both samples. However, the rms roughness of regrown AlN on PSEE (R_q : 0.082 nm) is much lower than that of conventional AlN (R_q : 0.135 nm). These results imply that the residual compressive strain of the AlN layer grown on the PSEE nanorod template was considerably relaxed by introducing voids, compared to that of conventional AlN.

In summary, we first demonstrated the AlN template with many voids using PSEE using the MOCVD system without any lithography process. A fully merged AlN layer with voids was obtained using epitaxial lateral overgrowth by the low V/III ratio and NH_3 pulsed epitaxy during the regrowth process. The role of voids in the AlN material was confirmed by TEM, HR-XRD, CL, Raman, and AFM measurements. The formation of voids in the AlN layer induced the enhancement of the crystal quality and relaxation of the residual strain in the AlN layer. In addition, the formation of voids is expected to enhance the LEE of the DUV LED by refracting the UV light emitted from the MQWs through further studies.

This work was supported by the KIST Institutional Program (Project No. 2E30100-20-039) and by the National Research Foundation of Korea (NRF) grant funded by the Korea Government (MSIT) (Grant No. 2020R1A4A4078674).

DATA AVAILABILITY

The data that support the findings of this study are available from the corresponding author upon reasonable request.

REFERENCES

- Y.-Y. Zheng, Y.-T. Ma, J.-Y. Zhang, and X. Xie, "COVID-19 and the cardiovascular system," *Nat. Rev. Cardiol.* **17**, 259 (2020).
- P. Mehta, D. F. McAuley, M. Brown, E. Sanchez, R. S. Tattersall, J. J. Manson, and HLH Across Speciality Collaboration, "COVID-19: Consider cytokine storm syndromes and immunosuppression," *Lancet* **395**, 1033 (2020).
- J. C. Rubio-Romero, M. d. C. Pardo-Ferreira, J. A. Torrecilla-García, and S. Calero-Castro, "Disposable masks: Disinfection and sterilization for reuse, and non-certified manufacturing, in the face of shortages during the COVID-19 pandemic," *Saf. Sci.* **129**, 104830 (2020).
- K. Song, M. Mohseni, and F. Taghipour, "Application of ultraviolet light-emitting diodes (UV-LEDs) for water disinfection: A review," *Water Res.* **94**, 341 (2016).
- A. Khan, K. Balakrishnan, and T. Katona, "Ultraviolet light-emitting diodes based on group three nitrides," *Nat. Photonics* **2**, 77 (2008).
- M. Kneissl, T.-Y. Seong, J. Han, and H. Amano, "The emergence and prospects of deep-ultraviolet light-emitting diode technologies," *Nat. Photonics* **13**, 233 (2019).
- K. Ban, J.-i. Yamamoto, K. Takeda, K. Ide, M. Iwaya, T. Takeuchi, S. Kamiyama, I. Akasaki, and H. Amano, "Internal quantum efficiency of whole-composition-range AlGaIn multiquantum wells," *Appl. Phys. Express* **4**, 052101 (2011).

- ⁸M. Shatalov, W. Sun, A. Lunev, X. Hu, A. Dobrinsky, Y. Bilenko, J. Yang, M. Shur, R. Gaska, C. Moe, G. Garrett, and M. Wraback, "AlGaIn deep-ultraviolet light-emitting diodes with external quantum efficiency above 10%," *Appl. Phys. Express* **5**, 082101 (2012).
- ⁹B. So, C. Cheon, J. Lee, J. Lee, T. Kwak, U. Choi, J. Song, J. Chang, and O. Nam, "Epitaxial growth of deep ultraviolet light emitting diodes with two-step *n*-AlGaIn layer," *Thin Solid Films* **708**, 138103 (2020).
- ¹⁰B. So, J. Kim, E. Shin, T. Kwak, T. Kim, and O. Nam, "Efficiency improvement of deep-ultraviolet light emitting diodes with gradient electron blocking layers," *Phys. Status Solidi A* **215**, 1700677 (2017).
- ¹¹B. So, J. Kim, T. Kwak, T. Kim, J. Lee, U. Choi, and O. Nam, "Improved carrier injection of AlGaIn-based deep ultraviolet light emitting diodes with graded superlattice electron blocking layers," *RSC Adv.* **8**, 35528 (2018).
- ¹²M. Katsuragawa, S. Sota, M. Komori, C. Anbe, T. Takeuchi, H. Sakai, H. Amano, and I. Akasaki, "Thermal ionization energy of Si and Mg in AlGaIn," *J. Cryst. Growth* **189-190**, 528 (1998).
- ¹³K. B. Nam, M. L. Nakarmi, J. Li, J. Y. Lin, and H. X. Jiang, "Mg acceptor level in AlN probed by deep ultraviolet photoluminescence," *Appl. Phys. Lett.* **83**, 878 (2003).
- ¹⁴M. Martens, C. Kuhn, E. Ziffer, T. Simoneit, V. Kueller, A. Knauer, J. Rass, T. Wernicke, S. Einfeldt, M. Weyers, and M. Kneissl, "Low absorption loss p-AlGaIn superlattice cladding layer for current-injection deep ultraviolet laser diodes," *Appl. Phys. Lett.* **108**, 151108 (2016).
- ¹⁵M. Imura, K. Nakano, G. Narita, N. Fujimoto, N. Okada, K. Balakrishnan, M. Iwaya, S. Kamiyama, H. Amano, I. Akasaki, T. Noro, T. Takagi, and A. Bandoh, "Epitaxial lateral overgrowth of AlN on trench-patterned AlN layers," *J. Cryst. Growth* **298**, 257 (2007).
- ¹⁶F. J. Xu, L. S. Zhang, N. Xie, M. X. Wang, Y. H. Sun, B. Y. Liu, W. K. Ge, X. Q. Wang, and B. Shen, "Realization of low dislocation density AlN on a small-coalescence-area nano-patterned sapphire substrate," *CrystEngComm* **21**, 2490 (2019).
- ¹⁷B. Tan, J. Hu, J. Zhang, Y. Zhang, H. Long, J. Chen, S. Du, J. Dai, C. Chen, J. Xu, F. Liu, and X. Li, "AlN gradient interlayer design for the growth of high-quality AlN epitaxial film on sputtered AlN/sapphire substrate," *CrystEngComm* **20**, 6557 (2018).
- ¹⁸C. He, W. Zhao, H. Wu, S. Zhang, K. Zhang, L. He, N. Liu, Z. Chen, and B. Shen, "High-quality AlN film grown on sputtered AlN/sapphire via growth-mode modification," *Cryst. Growth Des.* **18**, 6816 (2018).
- ¹⁹M. Conroy, V. Z. Zubialevich, H. Li, N. Petkov, J. D. Holmes, and P. J. Parbrook, "Epitaxial lateral overgrowth of AlN on self-assembled patterned nanorods," *J. Mater. Chem. C* **3**, 431 (2015).
- ²⁰Z. Y. Fan, G. Rong, N. Newman, and D. J. Smith, "Defect annihilation in AlN thin films by ultrahigh temperature processing," *Appl. Phys. Lett.* **76**, 1839 (2000).
- ²¹O.-H. Nam, M. D. Bremser, T. S. Zheleva, and R. F. Davis, *Appl. Phys. Lett.* **71**, 2638 (1997).
- ²²S.-M. Kim, K.-H. Lee, and G. Y. Jung, "Epitaxial lateral overgrowth on the air void embedded SiO₂ mask for InGaIn light-emitting diodes," *CrystEngComm* **15**, 6062 (2013).
- ²³D. Eom, J. Kim, K. Lee, M. Jeon, C. Heo, J. Pyeon, and O. Nam, "AlN nanostructures fabricated on a vicinal sapphire (0001) substrate," *Cryst. Growth Des.* **15**, 1242 (2015).
- ²⁴J. Kim, U. Choi, J. Pyeon, B. So, and O. Nam, "Deep-ultraviolet AlGaIn/AlN core-shell multiple quantum wells on AlN nanorods via lithography-free method," *Sci. Rep.* **8**, 935 (2018).
- ²⁵L. Zhang, F. Xu, J. Wang, C. He, W. Guo, M. Wang, B. Sheng, L. Lu, Z. Qin, X. Wang, and B. Shen, "High-quality AlN epitaxy on nano-patterned sapphire substrates prepared by nano-imprint lithography," *Sci. Rep.* **6**, 35934 (2016).
- ²⁶K. Lee, J. Kim, D. Eom, M. Jeon, C. Heo, J. Pyeon, and O. Nam, "Polarity of aluminum nitride layers grown by high-temperature metal organic chemical vapor deposition," *J. Nanosci. Nanotechnol.* **16**, 11807 (2016).
- ²⁷R. Kirste, S. Mita, L. Hussey, M. P. Hoffmann, W. Guo, I. Bryan, Z. Bryan, J. Tweedie, J. Xie, M. Gerhold, R. Collazo, and Z. Sitar, "Polarity control and growth of lateral polarity structures in AlN," *Appl. Phys. Lett.* **102**, 181913 (2013).
- ²⁸T. Y. Wang, J. H. Liang, G. W. Fu, and D. S. Wu, "Defect annihilation mechanism of AlN buffer structures with alternating high and low V/III ratios grown by MOCVD," *CrystEngComm* **18**, 9152 (2016).
- ²⁹A. V. Lobanova, K. M. Mazaev, R. A. Talalaev, M. Leys, S. Boeykens, K. Cheng, and S. Degroote, "Effect of V/III ratio in AlN and AlGaIn MOVPE," *J. Cryst. Growth* **287**, 601 (2006).
- ³⁰J. Bai, T. Wang, P. J. Parbrook, K. B. Lee, and A. G. Cullis, "A study of dislocations in AlN and GaN films grown on sapphire substrates," *J. Cryst. Growth* **282**, 290 (2005).
- ³¹B. Heying, X. H. Wu, S. Keller, Y. Li, D. Kapolnek, B. P. Keller, S. P. DenBaars, and J. S. Speck, "Role of threading dislocation structure on the x-ray diffraction peak widths in epitaxial GaN films," *Appl. Phys. Lett.* **68**, 643 (1996).
- ³²D. G. Zhao, D. S. Jiang, H. Yang, J. J. Zhu, Z. S. Liu, S. M. Zhang, J. W. Liang, X. Li, X. Y. Li, and H. M. Gong, "Role of edge dislocations in enhancing the yellow luminescence of n-type GaN," *Appl. Phys. Lett.* **88**, 241917 (2006).
- ³³D. Zhuang and J. Edgar, "Wet etching of GaN, AlN, and SiC: A review," *Mater. Sci. Eng.* **48**, 1 (2015).
- ³⁴Q. Paduano and D. Weyburne, "Optimized coalescence method for the metal-organic chemical vapor deposition growth of high quality Al-polarity AlN films on sapphire," *Jpn. J. Appl. Phys., Part 2* **44**, L150 (2005).
- ³⁵H. Long, J. Dai, Y. Zhang, S. Wang, B. Tan, S. Zhang, L. Xu, M. Shan, Z. C. Feng, H.-c. Kuo, and C. Chen, "High quality 10.6 μm AlN grown on pyramidal patterned sapphire substrate by MOCVD," *Appl. Phys. Lett.* **114**, 042101 (2019).
- ³⁶T. Koppe, H. Hofsäss, and U. Vetter, "Overview of band-edge and defect related luminescence in aluminum nitride," *J. Lumin.* **178**, 267 (2016).
- ³⁷T. Prokofyeva, M. Seon, J. Vanbuskirk, M. Holtz, S. Nikishin, N. Faleev, H. Temkin, and S. Zollner, "Vibrational properties of AlN grown on (111)-oriented silicon," *Phys. Rev. B* **63**, 125313 (2001).
- ³⁸S. Yang, R. Miyagawa, H. Miyake, K. Hiramatsu, and H. Harima, "Raman scattering spectroscopy of residual stresses in epitaxial AlN films," *Appl. Phys. Express* **4**, 031001 (2011).
- ³⁹C. B. Soh, H. Hartono, S. Y. Chow, S. J. Chua, and E. A. Fitzgerald, "Dislocation annihilation in regrown GaN on nanoporous GaN template with optimization of buffer layer growth," *Appl. Phys. Lett.* **90**, 053112 (2007).